Critical assessment of the validity of quasi-static pore network modeling in the application of underground hydrogen storage

Hashemi, Leila; Vuik, Cornelis

DOI
10.1016/j.advwatres.2024.104812

Publication date
2024

Document Version
Final published version

Published in
Advances in Water Resources

Citation (APA)
Hashemi, L., & Vuik, C. (2024). Critical assessment of the validity of quasi-static pore network modeling in the application of underground hydrogen storage. *Advances in Water Resources*, *193*, Article 104812. https://doi.org/10.1016/j.advwatres.2024.104812

Advances in Water Resources 193 (2024) 104812

Contents lists available at ScienceDirect

Advances in Water Resources

journal homepage: www.elsevier.com/locate/advwatres

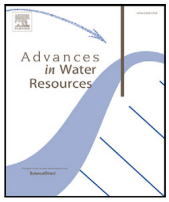

Critical assessment of the validity of quasi-static pore network modeling in the application of underground hydrogen storage

Leila Hashemi *, Cornelis Vuik

Faculty of Electrical Engineering, Mathematics and Computer Science, Department of Applied Mathematics, Delft University of Technology, Mekelweg 4, Delft, 2628 CD, The Netherlands

ARTICLE INFO

Keywords:
Underground hydrogen storage
Pore-network modeling
Dynamic and quasi-static

ABSTRACT

This study explores the suitability of quasi-static pore-network modeling for simulating the transport of hydrogen in networks with box-shaped pores and square cylinder throats. The dynamic pore-network modeling results are compared with quasi-static pore-network modeling, and a good agreement is observed when the simulations reach steady-state, for a capillary number of $N_c \leq 10^{-7}$. This finding suggests that the quasi-static approach can be used as a reliable and efficient method for studying hydrogen transport in similar networks.

1. Introduction

Underground Hydrogen Storage (UHS) in porous formations is a promising technology for large-scale (TWh) energy storage. To ensure the efficiency of the storage operation, multiscale modeling and simulation strategies are essential, in which the micro-scale physics are studied to derive input parameters for the continuum-scale dynamic models. In addition to pore-network modeling (Hashemi et al., 2021a), recent studies have employed direct numerical simulations and CFD modeling to analyze hydrogen–water flow dynamics. They highlighted the significance of these approaches in understanding the intricate flow behaviors (Wang et al., 2023; Bagheri et al., 2023). Therefore this study aims to extend the initial study of this complex process using quasi-static pore-network modeling (Hashemi et al., 2021a) and properly characterize the dynamics of the system. The present study uses a dynamic pore-network modeling (D-PNM) approach (Koch et al., 2021) to simulate the immiscible two-phase flow of hydrogen and water through a pore network model of a porous structure. The model input parameters are based on the experimentally obtained fluid–gas properties as presented in literature (Hashemi et al., 2021a). As for the rock, statistical pore network models are generated to mimic the digital network information which is based on 3D X-ray images of porous samples. To preserve the simulation stability, the D-PNM solves the transient multi-phase Stokes equations fully implicitly, for pressure and phase volume concentrations. Through several test cases, we analyze the transport characteristics of the hydrogen/water interface, especially the fingering and spreading physics. These results shed new light on how a representative continuum-scale model should be created to study the process at the field scale.

Pore network modeling

Large-scale numerical simulation of multi-phase flow in porous media is crucial for predicting various phenomena in hydrology, environmental engineering, and petroleum engineering. Accurate descriptions of macroscopic properties such as capillary pressures and relative permeabilities are necessary for numerical reservoir simulations of multi-phase flow (Bo et al., 2023). These properties can be measured by time-consuming and costly laboratory experiments, or alternatively, physically-based models can be developed to predict multi-phase flow at the pore scale and estimate these macroscopic properties at the macro-scale (Ryazanov et al., 2012).

To simulate multi-phase flow in porous media, an accurate pore space structure is required. This can be obtained from CT imaging (Blunt et al., 2013) or 3D reconstructions (Raoof and Hassanizadeh, 2010). Pore network modeling provides an effective tool for estimating macroscopic transport properties with arbitrary wetting conditions, making it an attractive option for numerical simulations of multi-phase flow. However, PNM has limitations in dealing with gas compressibility and fingering effects, which are crucial for accurately predicting hydrogen behavior during storage and recovery processes. For more detailed information about pore-network modeling and the effect of compressibility, readers are referred to the literature (Blunt, 2017; Bagheri et al., 2023), respectively. In pore network modeling, the pore space refers to the empty space within a porous material where fluids can flow or be stored. It is the network of interconnected voids or pores that characterize the porous structure of a material, such as a rock, soil, or membrane. The description of the pore space in pore

* Corresponding author.
E-mail addresses: L.Hashemi@tudelft.nl (L. Hashemi), C.Vuik@tudelft.nl (C. Vuik).

https://doi.org/10.1016/j.advwatres.2024.104812
Received 18 December 2023; Received in revised form 29 August 2024; Accepted 5 September 2024
Available online 7 September 2024

network modeling involves characterizing the geometry, topology, and connectivity of the pores within the material. This can be done using various techniques, such as imaging (Blunt et al., 2013), and statistical modeling (Raoof and Hassanizadeh, 2010). The resulting data can then be used to construct an equivalent model of the pore network, which can be used to simulate fluid flow and transport processes within the material. The pore space can be characterized by several parameters, such as the pore size distribution, the tortuosity of the pores, and the connectivity of the network. These parameters can have a significant impact on the fluid flow behavior and transport properties of the material, such as absolute and relative permeability, and capillarity. The detailed information can be found in literature (Dong and Blunt, 2009; Joekar-Niasar et al., 2010a) An accurate and detailed description of the pore space is crucial for understanding the transport and storage behavior of porous materials and for optimizing their performance in various applications, such as oil and gas recovery, water filtration, and energy storage.

The appropriate pore-scale model can be used by considering the existing flow regimes (Lenormand et al., 1988). Two main types of network modeling tools are defined by the flow regime: capillary-dominated and viscous-dominated. In the case of a low capillary number (Shams, 2018; Boujelben and McDougall, 2017; Piri and Blunt, 2005), N_c, which is defined as, $N_c = \frac{\mu u}{\sigma} \leq 10^{-5}$ where μ is viscosity, u is fluid velocity and σ is interfacial tension, the viscous forces are insignificant and the flow is governed by capillary forces. In this case, quasi-static network modeling can be applied. Otherwise, dynamic network modeling should be used where both viscous and capillary forces are accounted for. Given how important Nc is for determining the suitability of the quasi-static approach, it is essential to evaluate how well this model performs as conditions get close to this threshold. This evaluation is especially important since real-world situations might have Nc values close to 10^{-5}, which could impact the accuracy and usefulness of the model's predictions. For conditions where Nc exceeds this threshold, indicating a significant influence of viscous forces, dynamic network modeling should be employed. This study considers both quasi-static and dynamic PNM, providing a more comprehensive analysis of fluid dynamics across different flow regimes. Despite the limitations of the quasi-static model, it provides valuable insights into the pore-scale dynamics under capillary-dominated conditions. However, realistic subsurface conditions can often present scenarios where the capillary number approaches or exceeds this critical threshold. Therefore, it becomes important to assess the quasi-static model's validity and performance under varying conditions closer to this boundary.

Dynamic pore network models

Dynamic pore network models have become a powerful tool for understanding fluid behavior in porous media, allowing for the capture of changing fluid properties and pore structure over time (Koplik and Lasseter, 1985; Al-Gharbi and Blunt, 2005; Aghaei and Piri, 2015). While previous dynamic pore network models have used explicit or semi-implicit approaches, these had limitations in accurately capturing the complex behavior of the fluid flow. To overcome these limitations, researchers have developed new modeling approaches, such as fully implicit dynamic pore network models, which improve accuracy and provide greater insight into two-phase flow and phase change in porous media (Chen et al., 2020; Weishaupt and Helmig, 2021).

The behavior of residual fluids in porous media is an important topic of study with a range of applications, including oil recovery, groundwater management, carbon sequestration, and energy storage. Dynamic pore network modeling has been used in several studies to investigate residual fluid behavior in porous media (An et al., 2020; Gong et al., 2023; Li et al., 2017). For instance, Li et al. (2017) used dynamic pore network models to investigate the effect of heterogeneity on residual fluid configurations during the imbibition process. They found that heterogeneity significantly affects residual fluid configurations, and the spatial distribution of residual fluids is highly dependent on the degree of heterogeneity in the porous medium. Specifically, the study demonstrated that in more heterogeneous media, the residual fluid configurations tend to be more dispersed and less connected, which can lead to higher residual saturation levels. Conversely, in more homogeneous media, the residual fluids are more likely to form larger, continuous clusters, which can be more easily mobilized and displaced. Fluid configurations refer to the spatial arrangement and connectivity of the wetting and non-wetting phases within the pore space. It includes how the fluids occupy the pores and throats, the formation of ganglia or clusters of trapped fluid, and the overall distribution of these clusters throughout the porous medium. These configurations are crucial because they influence the efficiency of fluid displacement processes and the overall recovery of the injected or displaced phase.

Chen et al. (2020) presented a study that investigated various numerical modeling approaches and quantified their level of accuracy in dynamic pore-network modeling of two-phase flow and phase change in porous media. The study demonstrated the limitations of explicit and semi-implicit approaches and presented fully implicit approaches for dynamic pore network modeling.

Similarly, Weishaupt and Helmig (2021) presented a dynamic pore network model that used a fully implicit approach to simulate two-phase flow in porous media. The authors validated their model using a synthetic porous media structure and demonstrated its ability to accurately simulate complex fluid flow behavior.

Overall, these new modeling approaches offer promising ways to more accurately simulate the behavior of two-phase flow in porous media and provide greater insight into the underlying physics of fluid flow. They have potential applications in a range of fields, including the oil and gas industry, environmental science, and materials science. For more information on the dynamic pore network models, please refer to the Appendix, which includes Table A.1.

The structure of the paper is as follows. First, the methodology and simulation approach will be described. Then the numerical modeling results of the dynamic simulation for hydrogen-brine system are reported in comparison with the quasi-static modeling and air–water systems. In the following section, the results of cyclic modeling by using experimentally measured contact angles for the hydrogen-brine system are shown. Finally, concluding remarks are presented.

2. Materials and methods

The following section aims to provide a summary of the methodology that has been used in DuMux which is an open-source simulator for flow and transport in porous media (Weishaupt and Helmig, 2021). The readers for more detailed information are referred to this Weishaupt (2020).

2.1. Displacements and transport properties

In addition to characterizing the pore space, it is also important to understand the displacement and transport properties of fluids in porous media. Displacement refers to the movement of one fluid by another fluid in the pore space, and transport properties refer to the ability of fluids to move through the porous material.

Threshold capillary pressure

Threshold capillary pressure is an important parameter that affects displacement behavior in porous media. The threshold capillary pressures associated with each mechanism are explained below and illustrated in Fig. 1.

It is the minimum pressure required to initiate fluid displacement in a pore network. When fluid flows through a porous medium, the narrowest parts of the medium, known as pore throats, limit the rate of drainage. To pass through the throat, a minimum pressure, known as the entry capillary pressure, must be exceeded. This pressure is determined by the radius of curvature and the contact angle of the

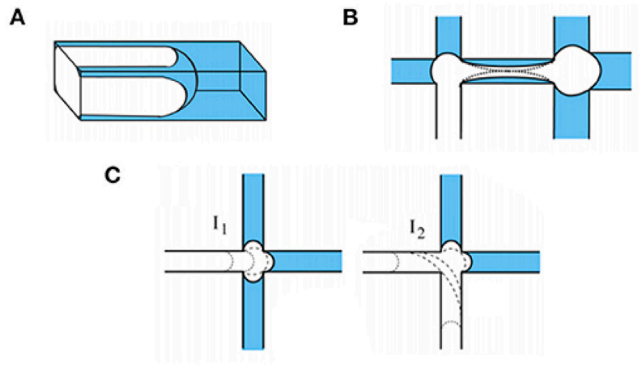

Fig. 1. The schematic diagram illustrates various processes in a rectangular tube: A. The drainage process is depicted using a piston-type displacement, where non-wetting phase is represented in white and wetting-phase in blue. B. The imbibition process showcases the snap-off phenomenon occurring in a pore-throat. C. Pore-body filling is illustrated, along with I1 and I2 events, during the imbibition process, again with non-wetting phase shown in white and wetting-phase shown in blue, I1 and I2 demonstrated cooperated pore-body filling with one and two pore throats filled with non-wetting-phase (Kohanpur et al., 2022).
Source: Adapted from Kohanpour et al.et al. (2022) under CC BY License.

phases. This pressure is calculated using the radius of the inscribed pore throat (r_{ij}) and the contact angle of the receding meniscus (θ_r). If the throat cross-section is circular, $p_{c,e}$ can be easily calculated using a simple formula. However, for non-circular throats, the calculation of $p_{c,e}$ is more complex and depends on the presence of wetting layers in the corners of the throat.

The entry capillary pressure for circular throat cross-sections is given by

$$p_{c,e} = \frac{2\gamma\cos(\theta_r)}{r_{ij}}, \tag{1}$$

where γ is the surface tension, θ_r is the receding contact angle, and r_{ij} is the inscribed radius of the pore throat connecting pore bodies i and j.

For angular throat cross sections, wetting layers may be present in the corners of the throat only if a certain condition is met, i.e.,

$$\beta + \theta_r < \frac{\pi}{2}, \tag{2}$$

where β is the corner half angle. For a rectangular throat with $\beta = \frac{\pi}{4}$, for instance, this means that the wetting phase can only be present in the corner if $\theta_r \leq \frac{\pi}{4}$ in order to keep a positive capillary pressure, i.e., a concave arc meniscus. The capillary pressure within that layer reads

$$p_c = \frac{\gamma}{r_{am}}, \tag{3}$$

where r_{am} is the radius of the arc meniscus.

For the irregular throat cross-sections, the entry capillary pressure can be derived analytically using the Mayer–Stowe–Princen (MSP) method (Patzek, 2001). The MSP method considers an energy balance for displacing the wetting phase and equates the curvature of the arc meniscus with that of the invading fluid's terminal meniscus. Blunt (Blunt, 2017) generalized this approach for arbitrary cross-sectional shapes, i.e.,

$$p_{c,e} = \frac{\gamma(1+2\sqrt{\pi G})\cos(\theta_r)F_d(\theta_r,G)}{r_{ij}}, \tag{4}$$

where G is the shape factor (the ratio of area to the square of the perimeter) of the cross-section and

$$F_d(\theta_r,G) = \frac{1+\sqrt{1+4GE/\cos^2(\theta_r)}}{1+2\sqrt{\pi G}}, \tag{5}$$

with

$$E = \pi - \frac{2}{3}\theta_r + 3\sin(\theta_r)\cos(\theta_r) - \frac{\cos^2(\theta_r)}{4G}. \tag{6}$$

The snap-off capillary pressure, also known as the snap-off threshold, refers to the pressure required to cause the sudden disconnection or snap-off of a fluid phase in a porous medium (Patzek, 2001). It is particularly relevant in the context of layer swelling, where the behavior of fluid phases in the porous medium is of interest. The snap-off capillary pressure can be calculated based on the geometry of the throats, which are narrow constrictions within the porous medium. Importantly, unlike other capillary pressure calculations, determining the snap-off capillary pressure does not require an energy balance analysis. This characteristic makes it a convenient parameter to study and analyze the behavior of fluids in porous media. If the advancing contact angle is less than the maximum value given in Eq. (7), spontaneous snap-off can occur.

$$\theta_{a,max} = \frac{\pi}{2} - \min(\beta_i) \tag{7}$$

where $\theta_{a,max}$ is the maximum advancing contact angle, β_i is the corner half angle.

Otherwise, imbibition is forced, and the threshold capillary pressure for this mechanism is calculated using Eq. (8):

$$\begin{aligned} E_1 &= \frac{\cos(\theta_a+\beta_i)}{\sin(\beta_i)} \\ r_{SO,ij} &= r\frac{\cot(\beta_i)+\cot(\beta_i)}{E_1^i+E_1^j} \\ P^e_{c,SO} &= \begin{cases} \frac{\gamma}{\min(r_{SOij})} & if \quad \theta_a \leq \theta_{a,max} \\ P_c^{max}\frac{\cos(\theta_a+\min(\beta_i))}{\cos(\theta_r+\min(\beta_i))} & if \quad \theta_{a,max} < \theta_a < \pi - \min(\beta_i) \\ P_c^{max}\frac{-1}{\cos(\theta_r+\min(\beta_i))} & if \quad \theta_a \geq \pi - \min(\beta_i) \end{cases} \end{aligned} \tag{8}$$

where θ_a is the advancing contact angle, β_i is the corner half angle, r_{SOij} is the curvature radius corresponding to snap-off mechanism, $P^e_{c,SO}$ is the threshold snap-off capillary pressure, P_c^{max} is the maximum capillary pressure at the end of drainage cycle. E_1 is just an intermediate coefficient to calculate r_{SOij}.

Local capillary-pressure saturation relationship

To accurately model pressure and saturation in pore-network models, a local capillary-pressure saturation relationship per pore body must be formulated. This relationship is often derived based on geometrical assumptions, as in the case of the cubic pore body i described by Joekar-Niasar et al. (2010a). They proposed a simplified relationship for this cubic pore body where the local saturation $S_{w,i}$ is related to the capillary pressure $p_{c,i}$ via Eq. (2.35), i.e.,

$$p_{c,i}(S_{w,i}) = \frac{2\gamma}{r_i(1-exp(-6.83S_{w,i}))}. \tag{9}$$

Meanwhile, a similar relationship for truncated octahedron can be found in the work of Joekar-Niasar and Hassanizadeh (2012).

Transport properties

Transport properties such as permeability and diffusivity are also critical in predicting fluid flow and transport in porous media. Permeability is a measure of how easily fluids can flow through a porous material, and diffusivity is a measure of how quickly a fluid can diffuse through the material. These properties can be influenced by the pore size distribution, connectivity, and tortuosity of the pore network (Blunt, 2017; Weishaupt, 2020).

Estimation of the macroscopic fluid transport properties, including absolute permeability, relative permeabilities of each phase, and capillary pressure; can be done through the entire pore network.

Absolute permeability is determined by simulation of single-phase flow on the fully saturated network and solving Darcy's law, i.e.,

$$K = \frac{\mu_p Q_{total,sp} L}{A(\Phi_{inlet} - \Phi_{outlet})}, \tag{10}$$

where μ_p is the viscosity of a single-phase p, and L and A are the length and cross-sectional area of the network, respectively. Imposing

a potential drop ($\Phi_{inlet} - \Phi_{outlet}$) at two parallel surfaces of the network creates $Q_{total,sp}$; total flow rate.

Therefore, the relative permeability of each phase can be calculated as

$$K_{rp} = \frac{Q_{tmp}}{Q_{tsp}}, \tag{11}$$

where Q_{tmp} is the flow rate of phase p in a multiphase flow and Q_{tsp} is the total flow rate .

To find the total flow rate, we use mass conservation at each pore body i, i.e.,

$$\Sigma_j q_{p,ij} = 0, \tag{12}$$

where j is used to refer to all pore throats connected to pore i and $q_{p,ij}$, is the flow rate from pore i through throat j.

The basic assumptions are considering incompressible fluid and ignoring viscous pressure drops compared to the capillary pressure. The volumetric flow rate between two pore bodies i and j is calculated by the Hagen–Poiseuille equation,

$$q_{p,ij} = \frac{g_{p,ij}}{L_{ij}}(\Phi_{p,i} - \Phi_{p,j}), \tag{13}$$

where L is the distance between the centers of the two connected pore bodies i and j. $g_{p,ij}$ is the flow conductance between the two pore bodies. For the detailed calculation of hydraulic conductance, readers are referred to these references of Blunt (2017) and Patzek and Silin (2001).

By solving a set of mass conservation nonlinear equations, pore body pressures and saturation of phases can be calculated.

2.2. Two-phase flow modeling

The two-phase flow in porous media can be modeled by a set of governing equations.

Dynamic PNM

Dynamic pore-network models take into account time-dependent phase displacement processes and are able to model non-equilibrium capillary pressure states while considering the fluid phases' viscosities. These models solve for pressure fields and phase fluxes based on mass or volume conservation, similar to conventional Darcy-type models. However, due to their highly non-linear behavior, dynamic models are computationally more complex and resource-intensive compared to quasi-static models (Blunt, 2017). The D-PNM solves the non-equilibrium state of two-phase flow in porous media. This means that transient behavior is involved. The pressure difference across the domain is not constant but varies over time due to fluid injection or withdrawal. Therefore, global pressure is not necessarily equal to local pressure at each time step.

Joekar-Niasar and Hassanizadeh (2012) extensively reviewed the different solution strategies for dynamic two-phase pore-network models. They classified dynamic models into two general types:

1. The first type assigns a single pressure to each pore body, assuming either the exclusive presence of a single phase or the concept of an equivalent pressure that accounts for both phases (Koplik and Lasseter, 1985; Mogensen and Stenby, 1998; Al-Gharbi and Blunt, 2005). While this approach reduces the computational complexity of the problem, Al-Gharbi and Blunt (2005) found inconsistencies with respect to equivalent quasi-static simulation results for networks with angular cross-sections.
2. The second type of algorithm used in this study is based on the two-pressure model, initially introduced by Thompson (Thompson, 2002). This model aims to solve for an individual pressure field for each phase and adopts a sequential solution strategy that decouples the pressure and saturation variables to accelerate the solution of the linearized problems. It bears a resemblance to the IMPES (implicit pressure, explicit saturation) method commonly employed in reservoir models.

In the two-pressure model, the algorithm first solves the pressures for each phase. This decoupling enables a faster solution but necessitates the use of small time steps to maintain numerical stability during the explicit saturation update. Although the two-pressure model demonstrated limitations in accurately capturing quasi-static results and was found to be unsuitable for very low capillary numbers (Ca) (Thompson, 2002), it provided valuable insights into the dynamics of multiphase flow in porous media.

To enhance the accuracy of the two-pressure model and address the highly non-linear nature of the processes, Joekar-Niasar et al. (2010b) proposed an improvement by introducing a semi-implicit saturation update. This enhancement allows for a better representation of complex multiphase flow behavior. Since then, this improved two-pressure model has been successfully applied in various studies (Qin et al., 2016; Khayrat and Jenny, 2016).

Governing Equations

In the two-pressure model, the following equations govern the flow unknowns:

(a) Conservation of mass for phase 1 (wetting phase)

$$\nabla \cdot (\rho_1 \mathbf{v}_1) = \frac{\partial}{\partial t}(\phi s_1 \rho_1) + \nabla \cdot (\phi s_1 \rho_1 \mathbf{v}_1) \tag{14}$$

(b) Conservation of mass for phase 2 (non-wetting phase)

$$\nabla \cdot (\rho_2 \mathbf{v}_2) = \frac{\partial}{\partial t}(\phi s_2 \rho_2) + \nabla \cdot (\phi s_2 \rho_2 \mathbf{v}_2) \tag{15}$$

(c) Darcy's law for phase 1 (wetting phase)

$$\mathbf{v}_1 = -\frac{k_{r1}}{\mu_1}\left(\nabla p_1 - \rho_1\, g \nabla z\right) \tag{16}$$

(d) Darcy's law for phase 2 (non-wetting phase)

$$\mathbf{v}_2 = -\frac{k_{r2}}{\mu_2}\left(\nabla p_2 - \rho_2\, g \nabla z\right) \tag{17}$$

(e) Capillary pressure-saturation relationship

$$p_c = p_1 - p_2 \tag{18}$$

These equations capture the pressure and saturation evolution and provide a foundation for simulating flow behavior in porous media using the two-pressure model.

Considering incompressible phases, mass conservation equations for the wetting and non-wetting phases read (Weishaupt, 2020):

$$V_i \frac{\partial S_i^w}{\partial t} + \sum_{j=1}^{N_i^j} Q_{ij}^w = Q_i^w, \tag{19}$$

$$V_i \frac{\partial S_i^n}{\partial t} + \sum_{j=1}^{N_i^j} Q_{ij}^n = Q_i^n, \tag{20}$$

where S_i^w and S_i^n represent the wetting and non-wetting phase saturations in pore i. V_i denotes the volume of pore i, while N_i^j represents the number of throats connected to pore i. Q_{ij}^w and Q_{ij}^n denote the flow rates of the wetting and non-wetting phases between pore i and throat j, respectively. Furthermore, Q_i^w and Q_i^n represent the total flow rates of the wetting and non-wetting phases in pore i, respectively.

The main difference between quasi-static and dynamic PNM is the inclusion of a time-related term in Eqs. (14) and (15). In the quasi-static approach, only mass conservation is considered by summing the flow rates into a pore body and there is no saturation change to the time.

The relationship between the wetting and non-wetting phase saturations reads:

$$S_i^w + S_i^n = 1. \tag{21}$$

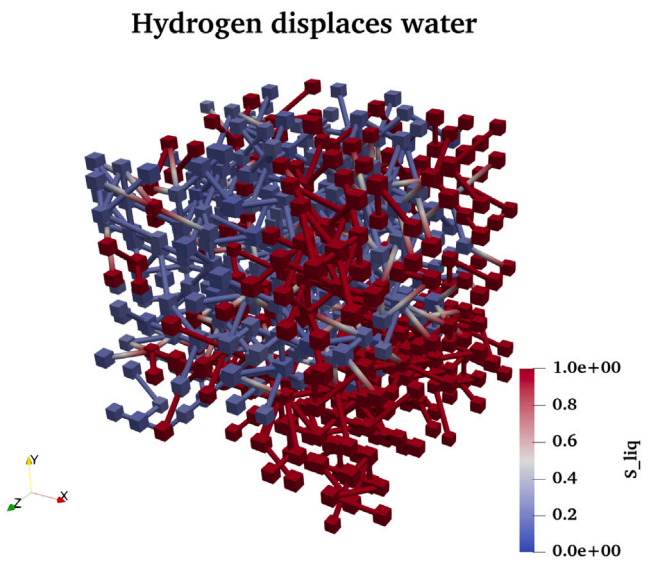

Fig. 2. Saturation distribution of hydrogen–water in a randomly generated network. S_{liq} in the color bar depicts the saturation of water.

The capillary pressure, P_c, can be defined as the pressure difference between the wetting and non-wetting phases, i.e.,

$$P_i^c = P_i^n - P_i^w. \tag{22}$$

This system is well-posed with four equations for the four unknowns ($S_i^n, S_i^w, P_i^w, P_i^n$), incorporating local rules to calculate capillary pressure, entry pressure, snap-off mechanism, and conductance.

DuMux, an open-source simulator for flow and transport in porous media, provides a platform for simulating and studying these phenomena. By utilizing a pore network model, DuMux enables the simulation of fluid flow and transport in porous media, allowing for the exploration of various parameter impacts on fluid behavior within the pore space. For further details on the simulation methodology, we refer to the Weishaupt and Helmig (2021) and Weishaupt (2020).

Simulation approach:

The simulation approach for dynamic PNM is a fully implicit method, which is used when pressure and saturation are strongly coupled, such as in low capillary number flows or unfavorable displacements ($M < 1$). The sequential coupling employed by IMPES and IMP-SIMS can pose numerical challenges in such cases. A fully implicit method ensures numerical stability by treating the pressure and saturation equations simultaneously.

To solve the system of equations using a fully implicit method, numerical schemes such as Newton–Raphson are used.

The fully implicit method enables the simultaneous solution of the pressure and saturation equations, enhancing numerical stability and capturing the strong coupling between pressure and saturation in low capillary number flows or unfavorable displacements.

In the next section, the results of the transport of hydrogen through a network with box-shaped pores and square cylinder throats using dynamic pore-network modeling are reported. The used network statistics, fluid and gas properties are summarized in Tables 1 and 2, respectively.

The average saturation of water in the network, denoted as $\langle S_w \rangle$, and the average capillary pressure, denoted as $\langle p_c \rangle$, were calculated using,

$$\langle S_w \rangle = \frac{\sum_i (S_w V)_i}{\sum_i V_i} \tag{23}$$

$$\langle p_c \rangle = \frac{\sum_i (S_n p_n V)_i}{\sum_i (S_n V)_i} - \frac{\sum_i (S_w p_w V)_i}{\sum_i (S_w V)_i}. \tag{24}$$

Table 1
The network statistics.
Source: Adapted from Weishaupt (2020).

Properties	values
Size (side length) [m]	1 E−3
Initial number. of pores	10 * 10 * 10
Probability deletion of the throat connections	90% for all spatial directions
Pore radius distribution	log-normal
Mean pore radius [m]	4.5 E−5
Standard deviation [m]	3 E−6

where S_w denotes the wetting phase saturation and V is the pore volume and p is the pressure of each phase. In the model, pore throats are assumed to be volumeless, serving only to control flow resistance, while the pore bodies are assumed to store the phases.

3. Results and discussion

The simulation results were compared with quasi-static pore-network modeling to assess the accuracy and reliability of the dynamic approach.[1]

The saturation of hydrogen–water in a randomly generated network is shown in Fig. 2, which illustrates the distribution of hydrogen–water saturation throughout the network.

The results of the modeling have been listed as follows.

- The dynamic simulation of hydrogen–water transport was compared with the quasi-static simulation, as shown in Fig. 3. A simulation starts with a fully saturated network with water, where the initial saturation is 1. In these simulations, the global capillary pressure is determined by applying a boundary pressure condition (BC) at each step. For each BC, the water saturation is calculated, and this is gradually increased to produce the P_c curve. The green line in Fig. 3 shows the global P_c curve from the dynamic simulation, connecting only the points where the system has reached equilibrium or steady-state. The yellow line represents the average dynamic P_c for each BC, which is calculated over time based on the governing Eqs. (23), (24). The red dashed line represents the global P_c curve from the quasi-static simulation, which inherently assumes steady-state conditions, resulting in a single P_c line.
  The simulation results showed a good agreement between the dynamic and quasi-static modeling approaches. When the dynamic simulation (yellow line) reaches a steady-state – defined here as the point where the saturation of hydrogen–water remains constant over time – the results of the dynamic (green circle marker) and the quasi-static (red dash-line) simulations match. This steady-state condition is characterized by no further changes in the saturation levels of the two phases. Before reaching steady state, the models show some differences due to transient effects (yellow line in Fig. 3), but these differences diminish as the system stabilizes. The match between these two methods indicates that the quasi-static simulation can be used as a reliable and efficient method for studying hydrogen transport in similar networks.
- The capillary pressure function of hydrogen–water against air–water was also analyzed, and the results are presented in Fig. 4.

[1] To replicate the results of this paper the source code can be accessed via this link https://git.iws.uni-stuttgart.de/dumux-pub/weishaupt2020a using the network information in Table 1 and the fluid and gas properties reported in Table 2.

Table 2
H_2-water and air–water properties used for Nc and M calculations.

Fluid properties	Depth	IFT (mN/m)	Viscosity_H_2 (Pa.s) *10^6	Viscosity_Brine (Pa.s) *10^6
H_2-Water (Yekta et al., 2018)	50 bar, 20 °C	51	8.94	999
	100 bar, 45 °C	46	9.54	597
Air-Water (Weishaupt, 2020)	Atmospheric	72.5	17.68	1000

- The behavior of hydrogen–water in the network was analyzed by calculating the Nc and M values for drainage and imbibition processes. M is a viscosity ratio and defines as, $M = \frac{\mu_{invadingphase}}{\mu_{defendingphase}}$. The relevant fluid properties and the calculated values are summarized in Table 2.
  The Nc and M calculations for drainage and imbibition of H_2-water, assuming a common velocity of 1 ft/day in the field are shown in Table 3.
- Additionally, a modified Lenormand diagram (Fig. 5) was used to illustrate the drainage and imbibition processes of hydrogen–water in the network. The diagram confirms that the system is still operating in the capillary-dominated regime, validating the use of the quasi-static pore network model.
- The sensitivity of this conclusion to different interfacial tensions has been analyzed and is illustrated in Fig. 6. This analysis demonstrates the expected effect of interfacial tension (IFT) on capillary pressure, showing an increase in capillary pressure with higher IFT values. Importantly, our findings remain consistent across the studied range of interfacial tensions. For a more comprehensive comparison, detailed plots contrasting the dynamic pore network model (DPNM) with the quasi-static pore network model (PNM) are provided in the Appendix.
- In continuation of the previous point, the quasi-static pore network model was employed using contact angles determined for H_2-Brine (Fig. 8). A comparison was made with previously presented P_c and Kr values obtained using different contact angles (receding contact angles of 21 and advancing contact angle of 85 degrees) (Fig. 7), as reported in our previous paper (Hashemi et al., 2021a). The static contact angle was determined through captive bubble experiments (Hashemi et al., 2021b), while the dynamic contact angles were measured using microfluidics experiments (van Rooijen et al., 2022). Both methods yielded intrinsic contact angles ranging from 25 to 45 degrees. The new results highlight a significant difference when direct contact angle measurements from the experimental work are utilized. This discrepancy is manifested in two main observations: firstly, a higher residual hydrogen saturation during production (secondary imbibition) compared to our previous paper (Hashemi et al., 2021a), and secondly, a higher relative permeability of water. These differences align with a lower gas–water contact angle and indicate a shift towards a more water-wet system.
- In continuation of the previous point, the quasi-static pore network model was employed using contact angles determined for H_2-Brine (Fig. 8). A comparison was made with previously presented P_c and Kr values obtained using different contact angles (Fig. 7), as reported in our previous paper (Hashemi et al., 2021a). The static contact angle was determined through captive bubble experiments (Hashemi et al., 2021b), while the dynamic contact angles were measured using microfluidics experiments (van Rooijen et al., 2022). Both methods yielded intrinsic contact angles ranging from 25 to 45 degrees. The new results highlight a significant difference when direct contact angle measurements from the experimental work are utilized. This discrepancy is manifested in two main observations: firstly, a higher residual hydrogen saturation during production (secondary imbibition) compared to our previous paper (Hashemi et al., 2021a),

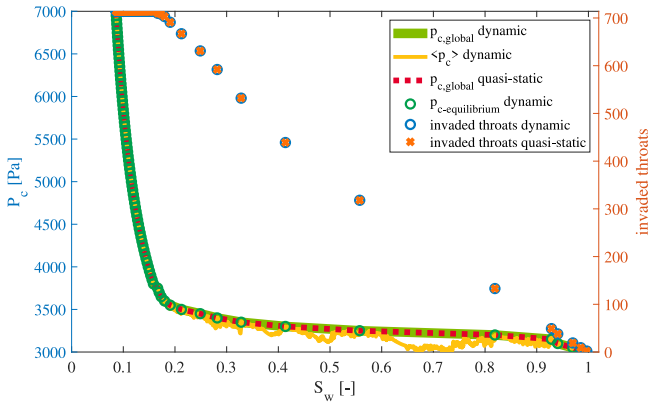

Fig. 3. Hydrogen–water dynamic simulation compared with static simulation. The left vertical axis shows the capillary pressure and in the right vertical access number of invaded throats is shown.

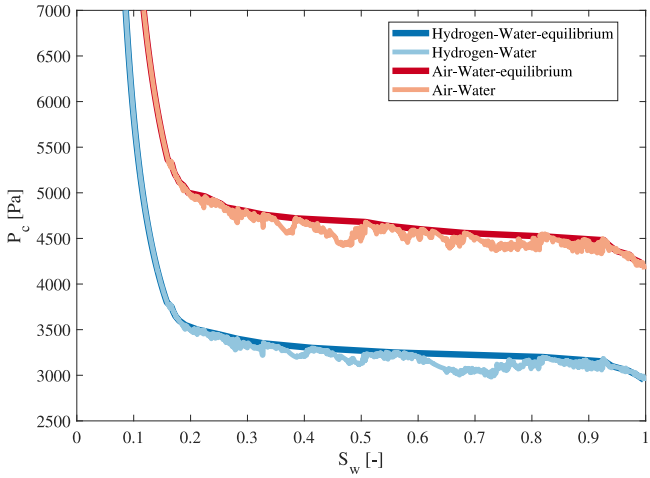

Fig. 4. Capillary pressure function of hydrogen/water against air–water.

and secondly, a higher relative permeability of water. These differences align with a lower gas–water contact angle and indicate a shift towards a more water-wet system.

Simulation Observations

The simulation results highlight several critical aspects of the trapping mechanisms during the two-phase flow, summarized as follows:

- **First Cycle — Primary Drainage**: In this process, only piston-like displacement is used for hydrogen to displace the water phase. Therefore, there is no discontinuity in the gas phase observed. Out of a total of 12,349 pores and 26,146 throats (excluding 118 isolated elements), 38,377 elements are invaded at the end of primary drainage, defining the irreducible water saturation of 0.24, which represents the clay volume as the trapped water phase.

Table 3
Calculated Nc and M for drainage and imbibition for H_2-water and air–water.

		Drainage				Imbibition			
Fluid properties	Depth	Nc	log (Nc)	M	log (M)	Nc	log (Nc)	M	log (M)
H_2-Water (Yekta et al., 2018)	50 bar, 20 °C	6.18E−10	−9.21	0.01	−2.05	6.910E−08	−7.16	111.74	2.05
	100 bar, 45 °C	7.32E−10	−9.14	0.02	−1.80	4.578E−08	−7.34	62.58	1.80
Air-Water (Weishaupt, 2020)	Atmospheric	8.60E−10	−9.07	0.02	−1.75	4.866E−08	−7.31	56.56	1.75

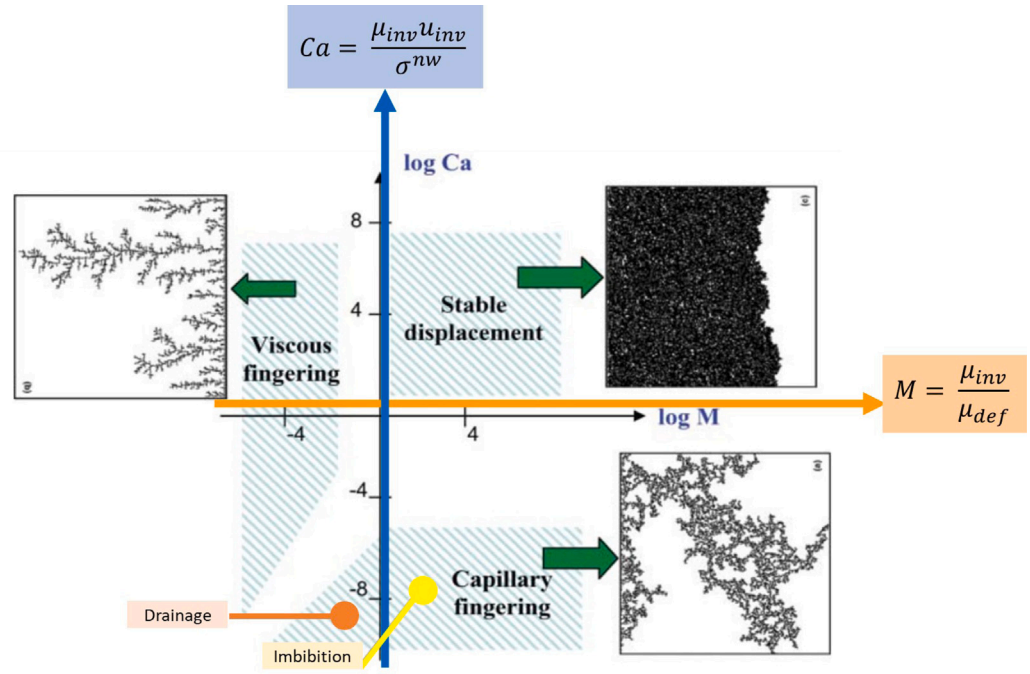

Fig. 5. Lenormand diagram with marked points for drainage and imbibition of H_2-water with the mentioned assumptions. Modified after (Joekar-Niasar et al., 2010b). Stable displacement refers to a flow regime where the invading fluid displaces the resident fluid uniformly, creating a stable front. This occurs when there is a balance between capillary and viscous forces. Viscous fingering occurs when the invading fluid creates finger-like patterns as it displaces the resident fluid, typically due to higher viscous forces compared to capillary forces. Capillary fingering is a regime where the displacement pattern is dominated by capillary forces, leading to irregular, branching pathways of the invading fluid.

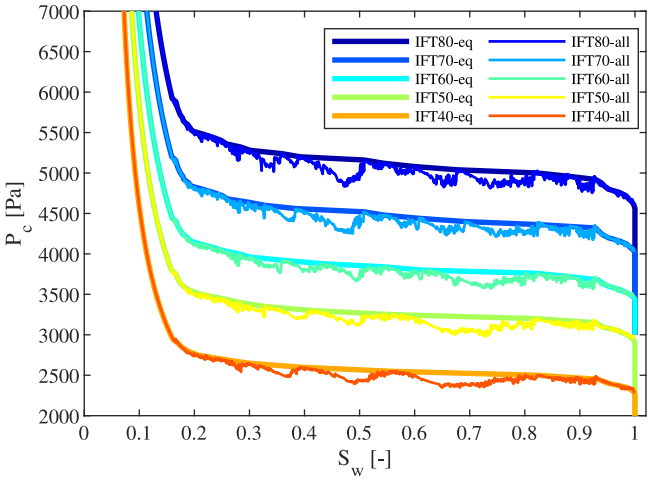

Fig. 6. Capillary pressure function of two-phase flow within the same network, with interfacial tensions ranging from 40 to 80 mN/m. 'eq' represents the equilibrium state of the DPNM, while 'all' shows the entire transition calculation of the DPNM.

- **Second Cycle — Secondary Imbibition**: This process is simulated considering the mechanisms mentioned in Fig. 1. There are 44 trapped water regions, including 108 elements, and 1757 trapped oil regions, including 10,466 elements. The pore and throat filling mechanisms are detailed as follows: during the pore filling process, there are 4956 uninvaded pores, 71 snap-off events, 3287 piston-type displacements, and 4035 pore body fillings (sum of I2, I3, and I4+). During the throat filling process, there are 5628 uninvaded throats, 10,297 snap-off events, and 10,221 piston-type displacements.
- **Third Cycle — Secondary Drainage**: This cycle reaches the same irreducible water saturation of 0.24. A total of 24,724 elements are invaded, and there are 2 regions of gas trapping.

3.1. Discussions

By utilizing the modified Lenormand diagram, the capillary-dominated regime of the system is reaffirmed, thereby supporting the use of the quasi-static pore network model. Furthermore, investigating the model with contact angles determined for H_2-Brine and comparing the results with previous findings reveals significant variations when different contact angle measurement methods are employed. These additions contribute to a comprehensive understanding of hydrogen–water behavior in the network and emphasize the importance of accurate contact angle measurements in simulations.

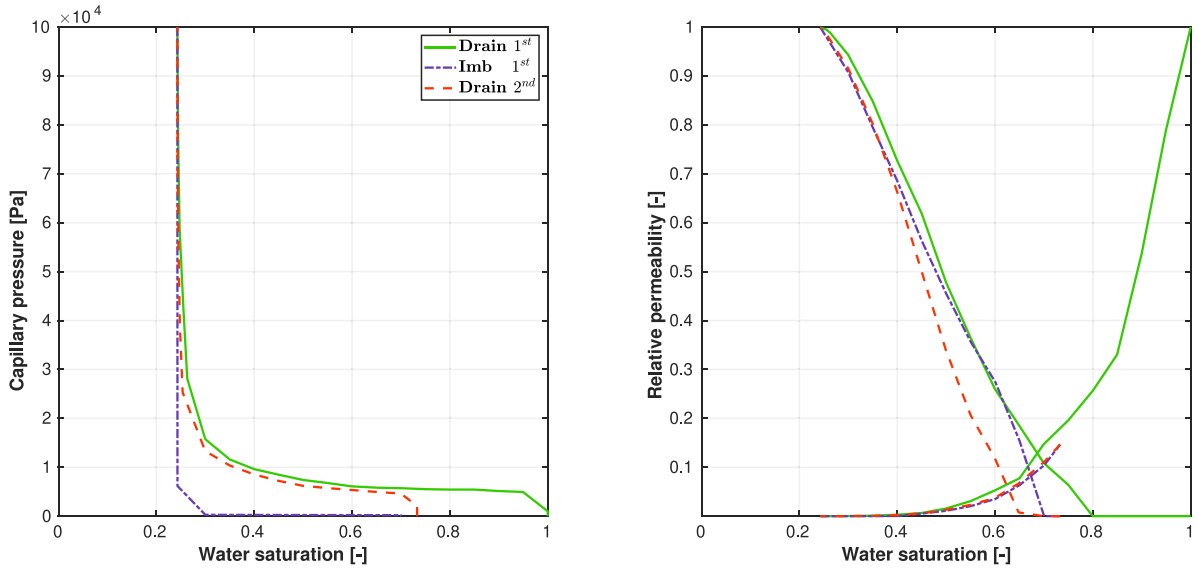

Fig. 7. Basecase simulation using Berea PNM reported in Hashemi et al. (2021a).

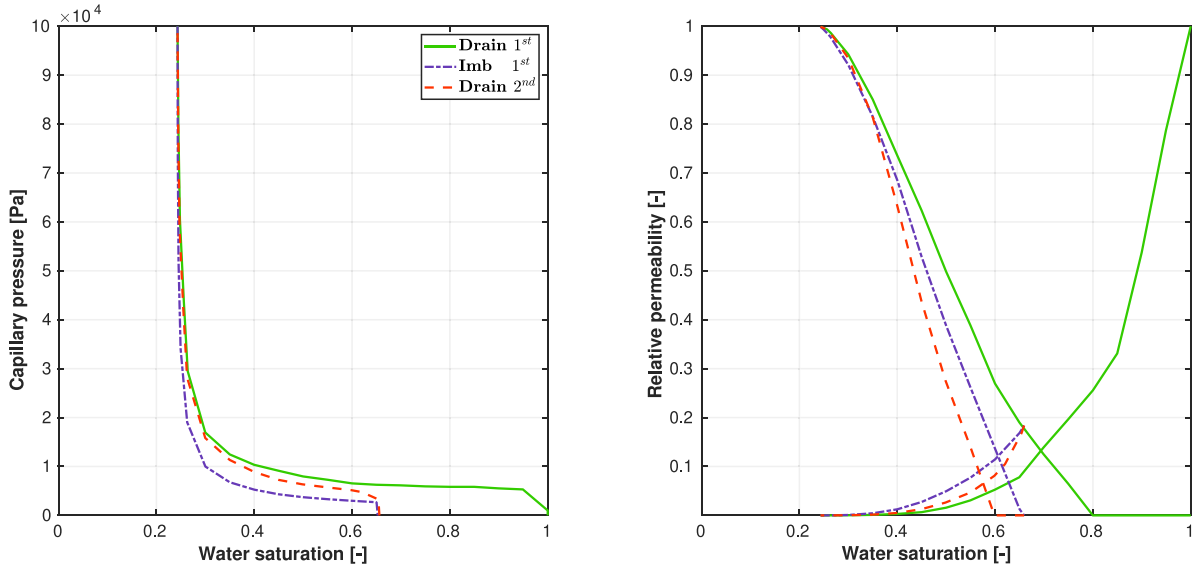

Fig. 8. Basecase simulation using Berea PNM and reported contact angles in Hashemi et al. (2021b).

It is worth addressing some assumptions related to the PNM approach and the differences in methodologies that cause the discrepancy between gas relative permeabilities at the end of the primary drainage cycle and the other reported experimental results in the literature, such as in these Boon and Hajibeygi (2022) and Yekta et al. (2018). The PNM assumes a simplified and idealized pore network, which does not capture the full complexity and heterogeneity of real porous media, often leading to an overestimation of gas flow efficiency once the non-wetting phase has been displaced. Additionally, PNM simulations apply specific boundary conditions and assume complete displacement during drainage, which might not fully represent experimental conditions where residual water saturation and dynamic boundary effects significantly influence results. Pore-scale phenomena such as snap-off, ganglia formation, and capillary pressure fluctuations are more accurately captured in experiments but are often oversimplified in PNMs, affecting the relative permeability outcomes. Finally, real porous media exhibit heterogeneity and anisotropy, which are often not fully represented in PNM, leading to an overestimation of gas permeability.

The results obtained from both dynamic and quasi-static pore-network modeling demonstrate a good match, suggesting that the use of quasi-static simulation is acceptable for hydrogen–water systems with smaller interfacial tension (IFT) values compared to air–water. This finding strengthens the validity of using quasi-static modeling

to capture the behavior of hydrogen–water in terms of the upscaled parameters of the P_c-S_w curve.

However, it is important to note that flow regimes based on the Lenormand diagram were conducted under the assumption of a common velocity in the field (Azin et al., 2021), which is a simplified representation that may not accurately reflect the complex flow patterns found in reality. As a suggestion for future work, it would be beneficial to relax this assumption and incorporate more realistic velocity fields into the modeling approach to gain a better understanding of the system dynamics.

Furthermore, the dynamic simulation utilized box-shaped pores and square cylinder throats, which may not capture the full range of pore and throat geometries encountered in real porous media. To enhance the generality of the model, it would be valuable to explore different pore and throat shapes and develop more generalized local rules that can accommodate various pore geometries.

Another limitation of the current dynamic simulation is the assumption of a non-zero contact angle. Incorporating contact angles into the simulation could provide more accurate results, as contact angles significantly influence fluid-fluid interactions at the pore scale. By considering contact angles, a more comprehensive understanding of the hydrogen–water system can be achieved.

Additionally, it is worth noting that the dynamic simulation only accounted for one cycle of displacement. Conducting simulations for multiple cycles of displacements would provide insights into the hysteresis phenomena associated with the hydrogen–water system, allowing for a more thorough investigation of the fluid displacement behavior and the impact of repeated cycles on the system.

Finally, the efficiency and scalability of the solver used for dynamic pore-network modeling are crucial considerations. Future research could explore strategies to improve the efficiency of the simulation without compromising accuracy, ensuring that large-scale simulations can be performed within reasonable timeframes. Additionally, scaling considerations should be taken into account to accurately represent field-scale conditions in the pore-network model.

Addressing these limitations and conducting further investigations based on the suggestions outlined above would enhance the understanding of the hydrogen–water system and contribute to the development of more robust and accurate simulation approaches for analyzing its behavior in porous media.

4. Conclusions

The study conducted a critical assessment of the validity of quasi-static pore network modeling (PNM) in the context of underground hydrogen storage. The results and discussions provided insights into the application of dynamic simulation in comparison to quasi-static PNM. The dynamic simulation results for the hydrogen–water system exhibited good agreement with the quasi-static PNM results, for capillary number $\leq 10^{-7}$ indicating that dynamic PNM is a valid approach for simulating hydrogen transport in these networks, as long as it reaches a steady state. The study also revealed that quasi-static simulation is acceptable for smaller interfacial tension (IFT) values compared to air–water, considering the upscaled parameters of the P_c-S_w curve.

Furthermore, the study identified several areas that require further research to enhance the validity of quasi-static PNM for hydrogen storage applications. These areas include exploring the scaling and size of the network, investigating different mechanisms, incorporating various pore and throat shapes, developing general local rules for different pore shapes, considering the influence of contact angles, and simulating additional cycles of displacements. Addressing these aspects will contribute to refining the accuracy and reliability of quasi-static PNM in simulating hydrogen storage systems.

Overall, the study emphasizes the importance of critically assessing modeling approaches to ensure the validity of simulation results in real-world applications like underground hydrogen storage.

CRediT authorship contribution statement

Leila Hashemi: Writing – original draft, Visualization, Modeling, Methodology, Conceptualization. **Cornelis Vuik:** Review & editing, Supervision, Methodology, Funding acquisition, Conceptualization.

Declaration of competing interest

The authors declare that they have no known competing financial interests or personal relationships that could have appeared to influence the work reported in this paper.

Data availability

Data will be made available on request.

Declaration of Generative AI and AI-assisted technologies in the writing process

During the preparation of this work the author(s) used Grammarly in order to improve language and readability. After using this tool/service, the author(s) reviewed and edited the content as needed and take(s) full responsibility for the content of the publication.

Acknowledgments

This study was conducted in DIAM (Delft Institute of Applied Mathematics) at Delft University of Technology. Prof. Hadi Hajibeygi is acknowledged for fruitful discussions during the development of this work. We gratefully thank Prof. Rainer Helmig for introducing their in-house open-source simulator of DuMux.

Appendix A. Dynamic pore network models

See Table A.1.

Appendix B. Additional simulation results

- The results of the different pore network models are summarized below. The properties of these networks are detailed in Table B.1 and visualized in Fig. B.1.
  The dynamic simulation of hydrogen–water transport was compared with the quasi-static simulation, as shown in Fig. B.2.
  The simulation results demonstrated a good agreement between the dynamic and quasi-static modeling approaches across different pore networks.
- The results of the simulations for the same pore network model (Fig. 2) for different interfacial tensions are summarized below. The corresponding computational costs are detailed in Table B.2 and comparison with quasi-static simulations visualized in Fig. B.3.
  All the simulation results demonstrated a good agreement between the dynamic and quasi-static modeling approaches using different IFT values.

Table A.1
Dynamic pore network models.

Year	Author(s)	Title	Ref.
1985	Koplik, Lasseter	Two-phase flow in random network models of porous media	Koplik and Lasseter (1985)
1988	Lenorman et al.	Numerical models and experiments on immiscible displacements in porous media	Lenormand et al. (1988)
1991	Blunt, King	Relative permeabilities from two-and three-dimensional pore-scale network modeling	Blunt and King (1991)
1996	Lee, Padmanabhan	Simulation of linear displacement experiments on massively parallel computers	Lee et al. (1996)
1996	Kamath et al.	Pore network modeling of laboratory experiments on heterogeneous carbonates	Kamath et al. (1996)
1997	van der Marck et al.	Viscous and capillary pressures during drainage: Network simulations and experiments	van der Marck et al. (1997)
1998	Mogensen, Stenby	A dynamic two-phase pore-scale model of imbibition	Mogensen and Stenby (1998)
1998	Aker et al.	A two-dimensional network simulator for two-phase flow in porous media	Aker et al. (1998)
1999	Dahle, Celia	A dynamic network model for two-phase immiscible flow	Dahle and Celia (1999)
2000	Hughes, Blunt	Pore-scale modeling of rate effects in imbibition	Hughes and Blunt (2000)
2002	Constantinides, Payatakes	Pore-scale modeling of fluid transport in disordered fibrous materials	Constantinides and Payatakes (2000)
2003	Singh, Mohanty	Dynamic modeling of drainage through three-dimensional porous materials	Singh and Mohanty (2003)
2003	Nordhaug	A pore network model for calculation of interfacial velocities	Nordhaug et al. (2003)
2005	Al-Gharbi, Blunt	Dynamic network modeling of two-phase drainage in porous media	Al-Gharbi and Blunt (2005)
2006	Nguyen et al.	The effect of displacement rate on imbibition relative permeability and residual saturation	Nguyen et al. (2006)
2006	Di Carlo	Quantitative network model predictions of saturation behind infiltration fronts and comparison with experiments	DiCarlo (2006)
2007	Piri, Karpyn	Prediction of fluid occupancy in fractures using network modeling and X-ray microtomography. ii: Results	Piri and Karpyn (2007)
2010a	Joekar et al.	Non-equilibrium effects in capillarity and interfacial area in two-phase flow: dynamic pore-network modeling	Joekar-Niasar et al. (2010a)
2010b	Joekar et al.	Network model investigation of interfacial area, capillary pressure, and saturation relationships in granular porous media	Joekar-Niasar et al. (2010b)
2011	Joekar, Hassanizadeh	Effect of fluids properties on non-equilibrium capillarity effects: Dynamic pore-network modeling	Joekar-Niasar and Hassanizadeh (2011a)
2011	Joekar, Hassanizadeh	Specific interfacial area: The missing state variable in two-phase flow equations?	Joekar-Niasar and Hassanizadeh (2011b)
2012	Joekar, Hassanizadeh	Analysis of fundamentals of two-phase flow in porous media using dynamic pore-network models: A review	Joekar-Niasar and Hassanizadeh (2012)
2012	Ellis, Bazylak	Dynamic pore network model of surface heterogeneity in brine-filled porous media for carbon sequestration,	Ellis and Bazylak (2012)
2012	Hammond, Unsal	A dynamic pore network model for oil displacement by wettability altering surfactant solution	Hammond and Unsal (2012)
2013	Sheng, Thompson	Dynamic coupling of pore-scale and reservoir-scale models for multiphase flow	Sheng and Thompson (2013)
2015	Aghaei, Piri	Direct pore-to-core up-scaling of displacement processes: Dynamic pore network modeling and experimentation	Aghaei and Piri (2015)
2015	Bagudu et al.	Pore-to-core-scale network modeling of co2 migration in porous media	Bagudu et al. (2015)
2016	Khayrat, Jenny	Subphase approach to model hysteretic two-phase flow in porous media	Khayrat and Jenny (2016)
2016	Huang et al.	Multi-physics pore-network modeling of two-phase shale matrix flows	Huang et al. (2016)
2016	Qin et al.	Pore-network modeling of water and vapor transport in the microporous layer and gas diffusion layer of a polymer electrolyte fuel cell	Qin et al. (2016)
2016	Cao et al.	Supercritical co2 and brine displacement in geological carbon sequestration: Micromodel and pore network simulation studies	Cao et al. (2016)
2016	Sheng, Thompson	A unified pore-network algorithm for dynamic two-phase flow	Sheng and Thompson (2016)
2017	Regaeig, Moncorge	Adaptive dynamic/quasi-static pore network model for efficient multiphase flow simulation	Regaieg and Moncorgé (2017)
2017	Li et al.	Dynamic pore-scale network model (PNM) of water imbibition in porous media	Li et al. (2017)
2017	Yang et al.	Pore to pore validation of pore network modeling against micromodel experiment results	Yang et al. (2017)
2017	Boujelben, McDougall	Dynamic pore-scale modeling of multiphase flow during application of eor techniques	Boujelben and McDougall (2017)
2018	Boujelben et al.	Pore network modeling of low salinity water injection under unsteady-state flow conditions	Boujelben et al. (2018)
2018	Gesho, et al.	Dynamic pore network modeling of two-phase flow through fractured porous media: Direct pore-to-core up-scaling of displacement processes	Gesho (2017)
2018	Gjennestad, et al.	Stable and efficient time integration of a dynamic pore network model for two-phase flow in porous media	Gjennestad et al. (2018)
2018	Sweijen et al.	Dynamic pore-scale model of drainage in granular porous media: The pore-unit assembly method	Sweijen et al. (2018)
2019	Qin et al.	A dynamic pore-network model for spontaneous imbibition in porous media	Qin and van Brummelen (2019)
2019	Qin et al.	Dynamic pore-network modeling of air–water flow through thin porous layers	Qin et al. (2019)
2019	Yin, et al.	Dynamic pore-network models development, in: Advances in Mathematical Methods and High-Performance Computing	Yin et al. (2019)
2019	Sinha et al.	A dynamic network simulator for immiscible two-phase flow in porous media	Sinha et al. (2019)
2020	Chen, Guo	Fully implicit dynamic pore-network modeling of two-phase flow and phase change in porous media	Chen et al. (2020)
2020	Gong and Piri	Pore-to-core upscaling of solute transport under steady-state two-phase flow conditions using dynamic pore network modeling approach	Gong and Piri (2020)
2021	Prmikulov et al.	Wettability and lenormand's diagram	Primkulov et al. (2021)

Table B.1
The network statistics of the 3 used models.

Properties	Main network (1)	Small network (2)	Network with smaller pores (3)
Size (side length) [m]	1 E−3	0.5 E−3	1 E−3
Initial number of pores	10 * 10 * 10	5 * 5 * 5	10 * 10 * 10
Probability deletion of the throat connections	90% for all spatial directions	Same	Same
pore radius distribution	log-normal	Same	Same
mean pore radius [m]	4.5 E−5	4.5 E−5	3 E−5
standard deviation [m]	3 E−6	Same	same
Cumulative CPU time (Dynamic) [s]	23804.5	2750.2	89015.7
Cumulative CPU time (Static) [s]	5	4	7

Table B.2
The corresponding computational cost of each dynamic simulation for different IFT.

IFT [mN/m]	40	50	60	70	80
Cumulative CPU time [s]	31417.82	23804.5	22406.7	18351.9	16353.5

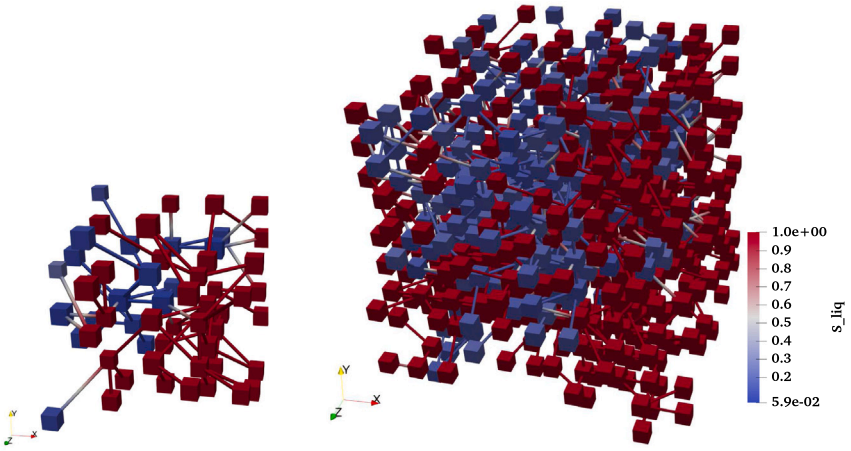

Fig. B.1. Saturation distribution of hydrogen–water in network number 2 (left) at a capillary pressure of 3880 Pa and network number 3 (right) at a capillary pressure of 4200 Pa.

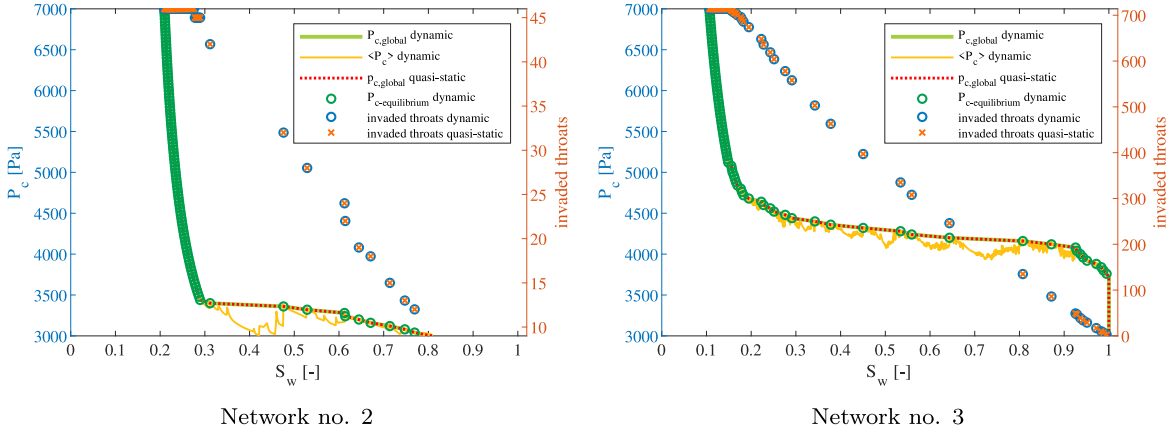

Fig. B.2. Hydrogen–water dynamic simulation compared with static simulation, using different networks.

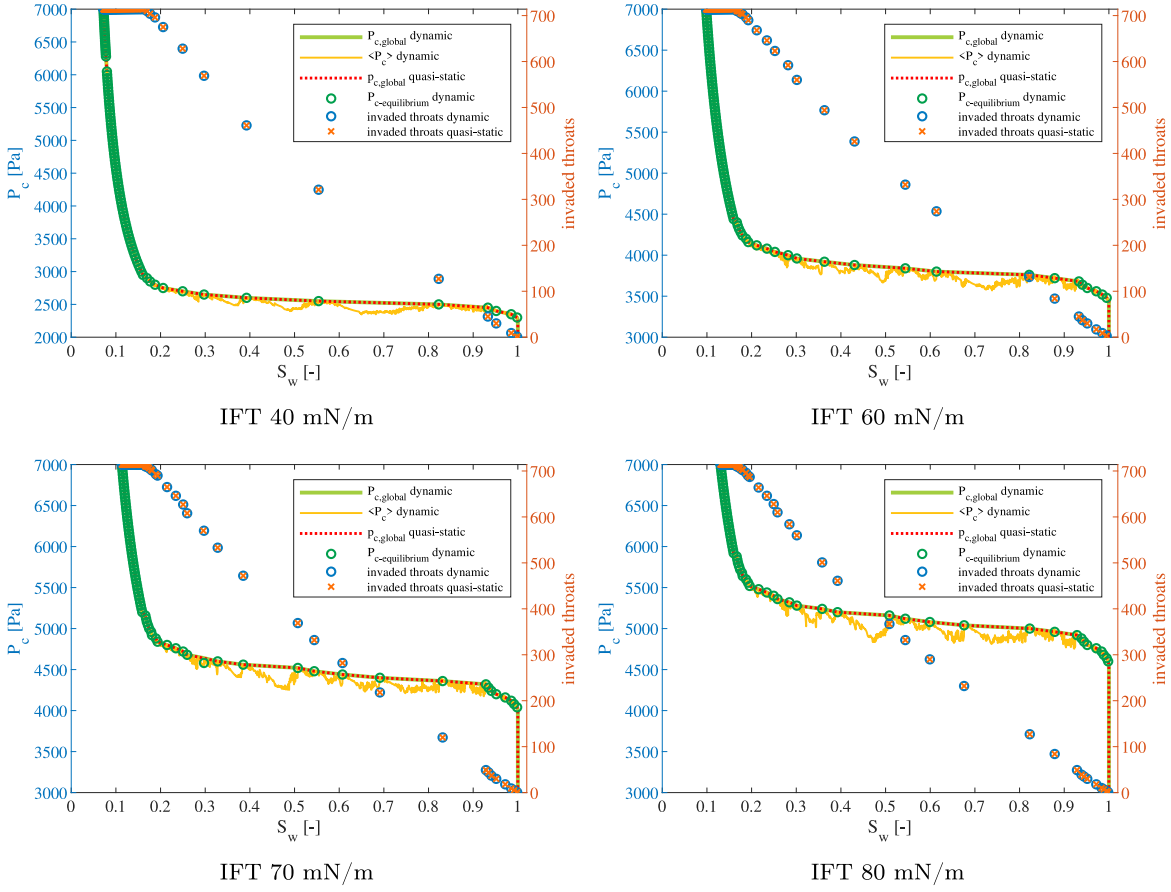

Fig. B.3. Hydrogen–water dynamic simulation compared with static simulation, using different IFT values.

References

Aghaei, A., Piri, M., 2015. Direct pore-to-core up-scaling of displacement processes: Dynamic pore network modeling and experimentation. J. Hydrol. 522, 488–509.

Aker, E., Måløy, K.J., Hansen, A., Batrouni, G.G., 1998. A two-dimensional network simulator for two-phase flow in porous media. Transp. Porous Media 32, 163–186.

Al-Gharbi, M.S., Blunt, M.J., 2005. Dynamic network modeling of two-phase drainage in porous media. Phys. Rev. E 71, 016308.

An, S., Erfani, H., Godinez-Brizuela, O.E., Niasar, V., 2020. Transition from viscous fingering to capillary fingering: Application of GPU-based fully implicit dynamic pore network modeling. Water Resour. Res. 56, e2020WR028149.

Azin, R., Izadpanahi, A., Zahedizadeh, P., 2021. Basics of oil and gas flow in reservoirs. In: Fundamentals and Practical Aspects of Gas Injection. pp. 73–142. http://dx.doi.org/10.1007/978-3-030-77200-0_3.

Bagheri, M., Mahani, H., Ayatollahi, S., Zivar, D., 2023. Direct pore-scale simulation of the effect of capillary number and gas compressibility on cyclic underground hydrogen storage & production in heterogeneous aquifers. Adv. Water Resour. 181, 104547. http://dx.doi.org/10.1016/j.advwatres.2023.104547, URL: https://www.sciencedirect.com/science/article/pii/S0309170823001811.

Bagudu, U., McDougall, S.R., Mackay, E.J., 2015. Pore-to-core-scale network modelling of CO_2 migration in porous media. Transp. Porous Media 110, 41–79.

Blunt, M.J., 2017. Multiphase Flow in Permeable Media: A Pore-Scale Perspective. Cambridge University Press.

Blunt, M.J., Bijeljic, B., Dong, H., Gharbi, O., Iglauer, S., Mostaghimi, P., Paluszny, A., Pentland, C., 2013. Pore-scale imaging and modelling. Adv. Water Resour. 51, 197–216.

Blunt, M., King, P., 1991. Relative permeabilities from two-and three-dimensional pore-scale network modelling. Transp. Porous Media 6, 407–433.

Bo, Z., Boon, M., Hajibeygi, H., Hurter, S., 2023. Impact of experimentally measured relative permeability hysteresis on reservoir-scale performance of underground hydrogen storage (UHS). Int. J. Hydrog. Energy.

Boon, M., Hajibeygi, H., 2022. Experimental characterization of [... formula...]/water multiphase flow in heterogeneous sandstone rock at the core scale relevant for underground hydrogen storage (UHS). Sci. Rep. 12.

Boujelben, A.H., McDougall, S.R., 2017. Dynamic pore scale modelling of multiphase flow during application of EOR techniques. In: 19th European Symposium on Improved Oil Recovery: Price World Sustainable IOR in a Low Oil.

Boujelben, A., McDougall, S., Watson, M., Bondino, I., Agenet, N., 2018. Pore network modelling of low salinity water injection under unsteady-state flow conditions. J. Pet. Sci. Eng. 165, 462–476.

Cao, S.C., Dai, S., Jung, J., 2016. Supercritical CO_2 and brine displacement in geological carbon sequestration: Micromodel and pore network simulation studies. Int. J. Greenh. Gas Control 44, 104–114.

Chen, S., Qin, C., Guo, B., 2020. Fully implicit dynamic pore-network modeling of two-phase flow and phase change in porous media. Water Resour. Res. 56, e2020WR028510.

Constantinides, G.N., Payatakes, A.C., 2000. Effects of precursor wetting films in immiscible displacement through porous media. Transp. Porous Media 38, 291–317.

Dahle, H.K., Celia, M.A., 1999. A dynamic network model for two-phase immiscible flow. Comput. Geosci. 3, 1–22.

DiCarlo, D.A., 2006. Quantitative network model predictions of saturation behind infiltration fronts and comparison with experiments. Water Resour. Res. 42.

Dong, H., Blunt, M.J., 2009. Pore-network extraction from micro-computerized-tomography images. Phys. Rev. E 80, 036307.

Ellis, J.S., Bazylak, A., 2012. Dynamic pore network model of surface heterogeneity in brine-filled porous media for carbon sequestration. Phys. Chem. Chem. Phys. 14, 8382–8390.

Gesho, M., 2017. Dynamic pore network modeling of two-phase flow through fractured porous media : Direct pore-to-core upscaling of displacement processes.

Gjennestad, M.A., Vassvik, M., Kjelstrup, S., Hansen, A., 2018. Stable and efficient time integration of a dynamic pore network model for two-phase flow in porous media. Front. Phys. 6, 56.

Gong, Y., Piri, M., 2020. Pore-to-core upscaling of solute transport under steady-state two-phase flow conditions using dynamic pore network modeling approach. Transp. Porous Media 135, 181–218.

Gong, Y., Sedghi, M., Piri, M., 2023. Dynamic pore-scale modeling of residual fluid configurations in disordered porous media. In: E3S Web of Conferences, vol. 366, p. 01018.

Hammond, P.S., Unsal, E., 2012. A dynamic pore network model for oil displacement by wettability-altering surfactant solution. Transp. Porous Media 92, 789–817.

Hashemi, L., Blunt, M., Hajibeygi, H., 2021a. Pore-scale modelling and sensitivity analyses of hydrogen-brine multiphase flow in geological porous media. Sci. Rep. 11, 8348.

Hashemi, L., Glerum, W., Farajzadeh, R., Hajibeygi, H., 2021b. Contact angle measurement for hydrogen/brine/sandstone system using captive-bubble method relevant for underground hydrogen storage. Adv. Water Resour. 103964.
Huang, X., Bandilla, K.W., Celia, M.A., 2016. Multi-physics pore-network modeling of two-phase shale matrix flows. Transp. Porous Media 111, 123–141.
Hughes, R.G., Blunt, M.J., 2000. Pore scale modeling of rate effects in imbibition. Transp. Porous Media 40, 295–322.
Joekar-Niasar, V., Hassanizadeh, S.M., 2011a. Effect of fluids properties on non-equilibrium capillarity effects: Dynamic pore-network modeling. Int. J. Multiph. Flow 37, 198–214.
Joekar-Niasar, V., Hassanizadeh, S.M., 2011b. Specific interfacial area: The missing state variable in two-phase flow equations? Water Resour. Res. 47.
Joekar-Niasar, V., Hassanizadeh, S.M., 2012. Analysis of fundamentals of two-phase flow in porous media using dynamic pore-network models: A review. Crit. Rev. Environ. Sci. Technol. 42, 1895–1976.
Joekar-Niasar, V., Hassanizadeh, S.M., Dahle, H.K., 2010a. Non-equilibrium effects in capillarity and interfacial area in two-phase flow: Dynamic pore-network modelling. J. Fluid Mech. 655, 38–71.
Joekar-Niasar, V., Prodanović, M., Wildenschild, D., Hassanizadeh, S.M., 2010b. Network model investigation of interfacial area, capillary pressure and saturation relationships in granular porous media. Water Resour. Res. 46.
Kamath, J., Xu, B., Lee, S.H., Yortsos, Y.C., 1996. Pore network modeling of laboratory experiments on heterogeneous carbonates. In: SPE Annual Technical Conference and Exhibition. OnePetro.
Khayrat, K., Jenny, P., 2016. Subphase approach to model hysteretic two-phase flow in porous media. Transp. Porous Media 111, 1–25.
Koch, T., Gläser, D., Weishaupt, K., et al., 2021. DuMux 3 – an open-source simulator for solving flow and transport problems in porous media with a focus on model coupling. Comput. Math. Appl. 81, 423–443.
Kohanpur, A.H., Chen, Y., Valocchi, A.J., 2022. Using direct numerical simulation of pore-level events to improve pore-network models for prediction of residual trapping of CO_2. Front. Water 3, 710160.
Koplik, J., Lasseter, T.J., 1985. Two-phase flow in random network models of porous media. Soc. Pet. Eng. J. 25, 89–100.
Lee, S.H., Padmanabhan, L., Al-Sunaidi, H.A., 1996. Simulation of linear displacement experiments on massively parallel computers. SPE J. 1, 327–340.
Lenormand, R., Touboul, E., Zarcone, C., 1988. Numerical models and experiments on immiscible displacements in porous media. J. Fluid Mech. 189, 165–187.
Li, J., McDougall, S.R., Sorbie, K.S., 2017. Dynamic pore-scale network model (PNM) of water imbibition in porous media. Adv. Water Resour. 107, 191–211.
van der Marck, S.C., Matsuura, T., Glas, J., 1997. Viscous and capillary pressures during drainage: Network simulations and experiments. Phys. Rev. E 56, 5675–5687, cited By 31.
Mogensen, K., Stenby, E.H., 1998. A dynamic two-phase pore-scale model of imbibition. Transp. Porous Media 32, 299–327.
Nguyen, V.H., Sheppard, A.P., Knackstedt, M.A., Pinczewski, W.V., 2006. The effect of displacement rate on imbibition relative permeability and residual saturation. J. Pet. Sci. Eng. 52, 54–70.
Nordhaug, H.F., Celia, M., Dahle, H.K., 2003. A pore network model for calculation of interfacial velocities. Adv. Water Resour. 26, 1061–1074.
Patzek, T.W., 2001. Verification of a complete pore network simulator of drainage and imbibition. SPE J. 6, 144–156.
Patzek, T.W., Silin, D.B., 2001. Shape factor and hydraulic conductance in noncircular capillaries: I. One-phase creeping flow. J. Colloid Interface Sci. 236, 295–304. http://dx.doi.org/10.1006/jcis.2000.7413, URL: http://www.sciencedirect.com/science/article/pii/S0021979700974137.
Piri, M., Blunt, M.J., 2005. Three-dimensional mixed-wet random pore-scale network modeling of two- and three-phase flow in porous media. I. Model description. Phys. Rev. E 71, 026301.
Piri, M., Karpyn, Z.T., 2007. Prediction of fluid occupancy in fractures using network modeling and X-ray microtomography. II: Results. Phys. Rev. E 76, 016316.
Primkulov, B.K., Pahlavan, A.A., Fu, X., Zhao, B., MacMinn, C.W., Juanes, R., 2021. Wettability and lenormand's diagram. J. Fluid Mech. 923.
Qin, C.-Z., van Brummelen, H., 2019. A dynamic pore-network model for spontaneous imbibition in porous media. Adv. Water Resour. 133, 103420.
Qin, C.-Z., Guo, B., Celia, M., Wu, R., 2019. Dynamic pore-network modeling of air-water flow through thin porous layers. Chem. Eng. Sci. 202, 194–207.
Qin, C.-Z., Hassanizadeh, S.M., Van Oosterhout, L.M., 2016. Pore-network modeling of water and vapor transport in the micro porous layer and gas diffusion layer of a polymer electrolyte fuel cell. Computation 4, 21.
Raoof, A., Hassanizadeh, S.M., 2010. A new method for generating pore-network models of porous media. Transp. Porous Media 81, 391–407.
Regaieg, M., Moncorgé, A., 2017. Adaptive dynamic/quasi-static pore network model for efficient multiphase flow simulation. Comput. Geosci. 21, 795–806.
van Rooijen, W., Hashemi, L., Boon, M., Farajzadeh, R., Hajibeygi, H., 2022. Microfluidics-based analysis of dynamic contact angles relevant for underground hydrogen storage. Advances in Water Resources 164, 104221.
Ryazanov, A., et al., 2012. Pore Scale Network Modelling of Residual Oil Saturation in Mixed-Wet Systems (Ph.D. thesis). Heriot-Watt University.
Shams, M., 2018. Modelling two-phase flow at the micro-scale using a volume-of-fluid method.
Sheng, Q., Thompson, K., 2013. Dynamic coupling of pore-scale and reservoir-scale models for multiphase flow. Water Resour. Res. 49, 5973–5988.
Sheng, Q., Thompson, K., 2016. A unified pore-network algorithm for dynamic two-phase flow. Adv. Water Resour. 95, 92–108.
Singh, M., Mohanty, K.K., 2003. Dynamic modeling of drainage through three-dimensional porous materials. Chem. Eng. Sci. 58, 1–18.
Sinha, S., Gjennestad, M.A., Vassvik, M., Hansen, A., 2019. A dynamic network simulator for immiscible two-phase flow in porous media. arXiv preprint arXiv:1907.12842.
Sweijen, T., Hassanizadeh, S.M., Chareyre, B., Zhuang, L., 2018. Dynamic pore-scale model of drainage in granular porous media: The pore-unit assembly method. Water Resour. Res. 54, 4193–4213.
Thompson, K.E., 2002. Pore-scale modeling of fluid transport in disordered fibrous materials. AIChE J. 48, 1369–1389.
Wang, J., Yang, Y., Cai, S., Yao, J., Xie, Q., 2023. Pore-scale modelling on hydrogen transport in porous media: Implications for hydrogen storage in saline aquifers. Int. J. Hydrog. Energy 48, 13922–13933. http://dx.doi.org/10.1016/j.ijhydene.2022.11.299, URL: https://www.sciencedirect.com/science/article/pii/S0360319922056415.
Weishaupt, K., 2020. Model Concepts for Coupling Free Flow with Porous Medium Flow at the Pore-Network Scale: From Single-Phase fFlow to Compositional Non-Isothermal Two-Phase Flow. Eigenverlag des Instituts fur Wasser-und Umweltsystemmodellierung ..., Stuttgart.
Weishaupt, K., Helmig, R., 2021. A dynamic and fully implicit non-isothermal, two-phase, two-component pore-network model coupled to single-phase free flow for the pore-scale description of evaporation processes. Water Resour. Res. 57, e2020WR028772.
Yang, J., Bondino, I., Regaieg, M., Moncorgé, A., 2017. Pore to pore validation of pore network modelling against micromodel experiment results. Comput. Geosci. 21, 849–862.
Yekta, A.E., Manceau, J.C., Gaboreau, S., Pichavant, M., Audigane, P., 2018. Determination of hydrogen–water relative permeability and capillary pressure in sandstone: Application to underground hydrogen injection in sedimentary formations. Transp. Porous Media 122, 333–356. http://dx.doi.org/10.1007/s11242-018-1004-7.
Yin, X., de Vries, E.T., Raoof, A., Hassanizadeh, S.M., 2019. Dynamic pore-network models development. In: Advances in Mathematical Methods and High Performance Computing. Springer, pp. 337–356.